Fabrication and characterization of a high performance NIR 2kx2k MCT array at CEA and Lynred for astronomy applications

Olivier Gravrand, Clément Lobre, Jean-Louis L Santailler, Titouan Le Goff, Nicolas Olivier Baier, Giacomo Badano, Olivier Boulade, Thibault Pichon, Alix Nouvel de la Fleche, Diane Sam-Giao, et al.

Fabrication and characterization of a high performance NIR 2kx2k MCT array at CEA and Lynred for astronomy applications

Olivier Gravrand, Clément Lobre, Jean-Louis Santailler, Titouan Legoff, Nicolas Baier, et al.

Olivier Gravrand, Clément Lobre, Jean-Louis Santailler, Titouan Legoff, Nicolas Baier, Giacomo Badano, Olivier Boulade, Thibault Pichon, Alix Nouvel-Delaflèche, Diane Sam Giao, Alexandre Maltere, Sébastien Aufranc, Frédéric Salvetti, Julien Roumegoux, Benoit Brosse, Adrien Lamoure, "Fabrication and characterization of a high performance NIR 2kx2k MCT array at CEA and Lynred for astronomy applications," Proc. SPIE 12107, Infrared Technology and Applications XLVIII, 1210706 (27 May 2022); doi: 10.1117/12.2618857

SPIE.

Event: SPIE Defense + Commercial Sensing, 2022, Orlando, Florida, United States

Fabrication and characterization of a high performance NIR 2kx2k MCT array at CEA and Lynred for astronomy applications

O. Gravrand[1*], O. Boulade[2], C. Lobre[1], J. L. Santailler[1], T. Legoff[1], T. Pichon[2], A. Nouvel De la Flèche[3], N. Baier[1], G. Badano[1], D. San Giao[4], A. Maltere[4], S. Aufranc[4], F. Salvetti[4], J. Roumegoux[4], B. Brosse[4] , A. Lamoure[4]

* olivier.gravrand@cea.fr

1. Univ. Grenoble Alpes, CEA, Leti, F-38000 Grenoble, France
2. CEA-IRFU, 27 av des martyrs, 38054 Grenoble, France
3. IRAP, 9 Av. du Colonel Roche, 31400 Toulouse, France
4. LYNRED, 364 av de Valence, 38113 Veurey Voroize, France

ABSTRACT

For several years now, LYNRED, CEA-LETI and CEA-IRFU have been involved in the development of large area, very high performance NIR retinas for astronomy, in the context of the ALFA program (Astronomical Large Format Array). It aims at demonstrating the ability to produce in Europe low flux 2kx2k arrays exhibiting the very high performances required by science applications. In this context, high performance means very low dark current (below 0.1 e/s/px) with high QE (above 80%). LETI and LYNRED succeeded this year in the fabrication of a 2kx2k array, with very high uniformity as characterized at IRFU. One of those arrays will be used on the CAGIRE camera of the SVOM mission, aiming at observing afterglows of gamma ray bursts. Additional studies are ongoing on test arrays manufactured with the same technology to assess the behavior of this technology in terms of persistence and radiation hardness for space use.

Keywords: NIR, MCT, low flux, SFD, 2kx2k

1. INTRODUCTION

The HgCdTe (MCT) material system is well known to provide the high QE as well as very the low dark current required for astronomical applications [1]. The ALFA (Astronomical Large Format Array) program aims at demonstrating the feasibility of large sensor array in NIR for astronomical need. The targeted format is 2kx2k arrays with 15µm pixel pitch and a 2.1µm cutoff wavelength at an operating temperature of 100K. The program is funded by ESA (NIRLFSA program) and French National Research Agency (ANR Labex FOCUS). This work relied also on Europe H2020 funding (Asteroid project), to go beyond a feasibility demonstration and drive the technology toward an industrial production line. Aside from the very high performances required for astronomical observations, the scaling from standard formats (TV 15µm pitch) to the larger format $2k \times 2k$ represents a serious challenge: the performance must be uniformly maintained on a $3 \times 3cm^2$ area (instead of the standard 1cm² chip area that represents most of our standard produced chips). This paper aims at presenting our progress in the manufacturing and characterization of such large format arrays for astronomy.

Infrared Technology and Applications XLVIII, edited by Bjørn F. Andresen, Gabor F. Fulop, Lucy Zheng
Proc. of SPIE Vol. 12107, 1210706 · © 2022 SPIE · 0277-786X · doi: 10.1117/12.2618857

2. ROIC DESCRIPTION AND DETECTOR TECHNOLOGY

Si readout integrated circuits (ROIC) used for such low flux detection are using a source follower per detector input stage (SFD) where the photodiode node is connected to the MOS gate as illustrated in Figure 1. In this configuration, generated photo-charges are integrated onto the diode capacitance itself and the useful signal is therefore the photodiode bias drift, measured using a readout MOS mounted as a source follower amplifier [2]. Such an architecture allows for non-destructive readings of very low signals, very suitable to low flux applications. Additional capacitance to the diode capacitance may be added using the Si input node to manage larger dynamics.

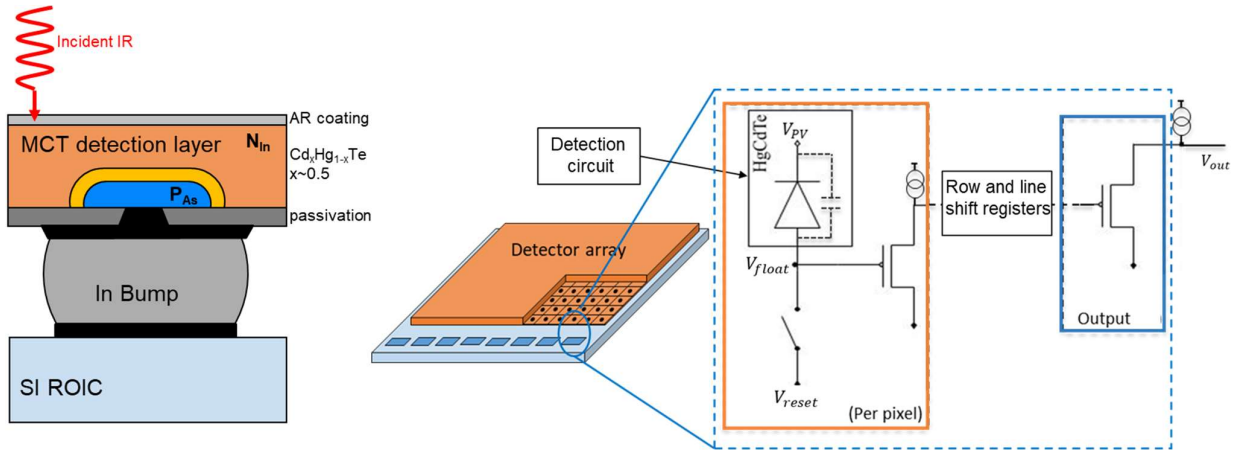

Figure 1: ALFA-Asteroid ROIC and diode schematics

A first ROIC available was a small format study ROIC (TV format, 15µm pitch and 4fF additional integration capacitance). This ROIC has been extensively used for technology diagnostic during the MCT process design phase, but also for the industrialization phase. The final version of the ROIC is a 2048x2048 format, 15µm pitch array using the same kind of input stage. For this ROIC, an additional 27fF capacitance was added on the Si input node to the diode capacitance, in order to increase the pixel linear dynamic. The ROIC design was also optimized in order to minimize as much as possible electroluminescence from the circuit (ROIC glow potentially polluting dark images). Such 2kx2k ROICs are then hybridized to MCT detection arrays using Indium bump and fully packaged at Lynred. Figure 2 gives a picture of the fully package $2k \times 2k$ focal plane array, with the large 3×3 cm² MCT ALFA chip. Final performances of the 2kx2k array are measured at CEA-IRFU.

This paper will not focus on ROIC features and performance. However, the focus will be given to the MCT diode performances. The fabrication of the detection layer was performed at CEA-LETI using our classical p/n technology [3]. Starting from lattice matched CdZnTe substrate, the MCT narrow gap active layer is grown using liquid phase epitaxy (LPE), introducing extrinsic N type doping (In). The resulting layer is then implanted with As followed by an activation annealing under Hg overpressure. The layer is finally passivated and contacted before hybridization onto the ROIC. Figure 1 left gives a schematic of the resulting final structure.

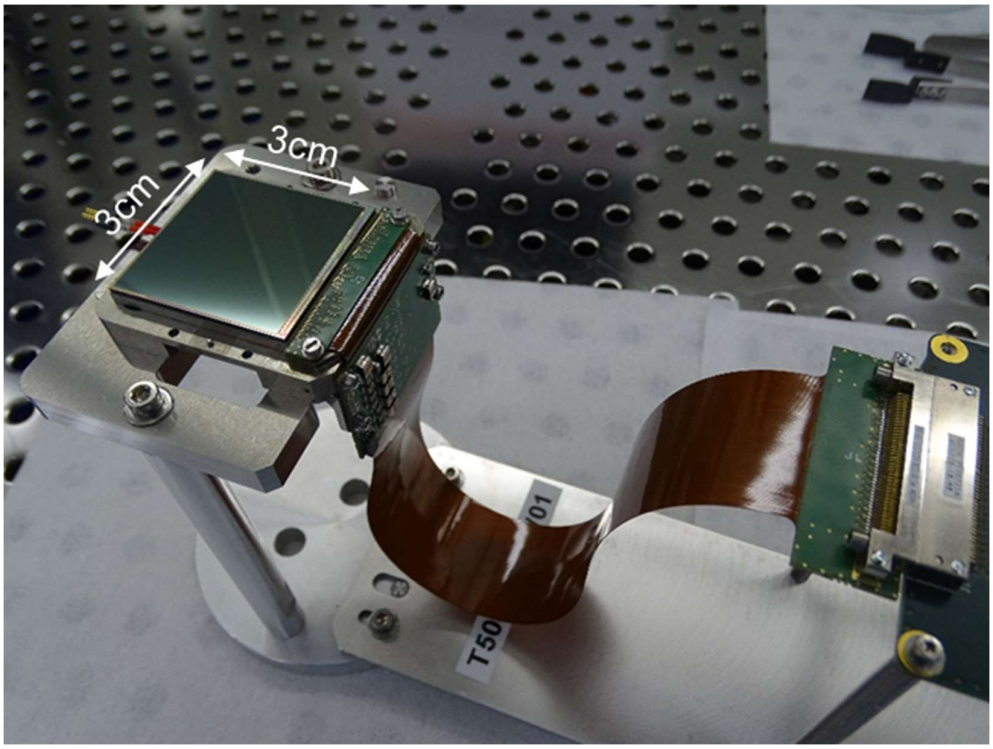

Figure 2: Fully packaged 2048 × 2048 *ALFA array*

3. QE AND RESPONSE UNIFORMITY

The first parameters presented here are flux related performances. The arrays were mounted into a low flux cryostat at CEA-IRFU, and cooled down to 100K. The cryostat is equipped with a small black body (BB) inside the cold chamber. Even if the distance from the BB to the detector is relatively large (11 cm), it does not ensure a perfect uniform illumination onto the 2kx2k ALFA detector area. However, varying the temperature of this BB allows flux variation and thus allows the investigation of the detector behavior of each pixel vs flux. The cryostat is also equipped with an optical fiber connecting the cold chamber to an external monochromator, in order to investigate the spectral properties of the pixels.

The rigorous quantification of the quantum efficiency (QE) as well as the response itself requires the accurate knowledge of the integration capacitance, i.e. the transimpedance gain. However, the charges being mostly integrated onto the diode capacitance itself, the effective value of the integration capacitance is not easily accessible. A popular method to estimate this capacitance involves the kTC rest noise. Measuring this reset noise at a given temperature T leads to a simple estimation of the integration capacitance C. Figure 3 show the resulting capacitance histogram for the ALFA detector, exhibiting a relatively narrow distribution shape peaking at 47.8fF, as expected from the diode capacitance and additional node capacitance from the ROIC.

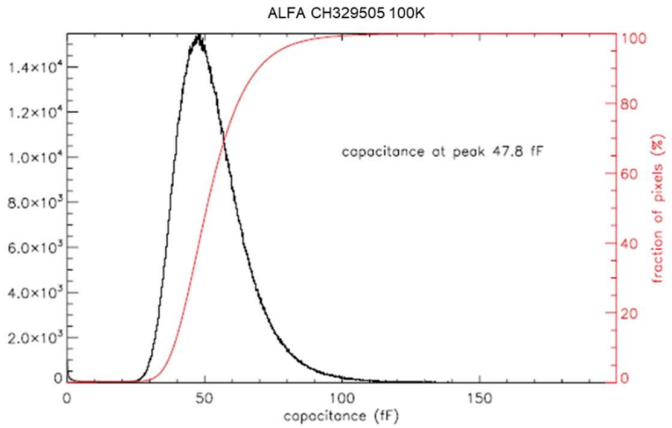

Figure 3: Estimation of the integration capacitance of the ALFA device at 100K, using kTC noise

When integrating flux, the output signal of each pixel of the array typically evolves as shown in Figure 4 left. The collected charges progressively fill the integration capacitance and the output signal varies until saturation (frame 100 and higher in the example of Figure 4). For an ideal capacitance, the evolution of this output signal before saturation should be linear. However, in the case of a diode capacitance, the capacitance value may not be perfectly linear: the capacitance (thus the pixel gain) may vary with the applied bias i.e. with the output signal. This induces nonlinear integration ramps, which have to be characterized. Given our previous estimation of the pixel capacitance, it is possible to translate the output signal of the integration ramp in V into integrated e- and then compute a non-linearity from 0 to 125ke- (ESA requirement was 60ke-). Figure 4 right gives the result of such an estimation for the ALFA device at 100K. The figure shows an histogram of this non-linearity for the 4Mpx. It exhibits a nice Gaussian shape centered at 0.43%, which is very low.

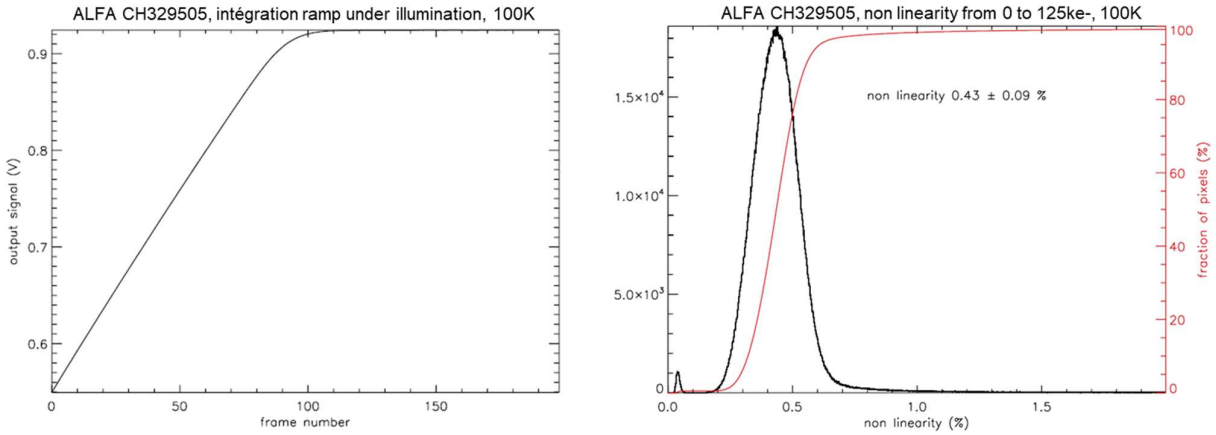

Figure 4: Estimation of the linearity of the ALFA device at 100K
Left: Typical integration ramp under illumination $T_{frame} = 1.3s$)
Right : non linearity histogram from 0 to 125ke-

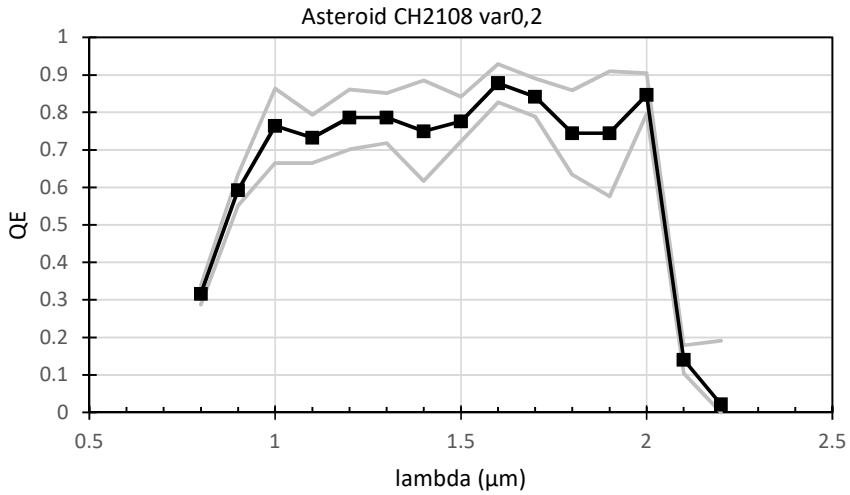

Figure 5: Spectral QE measured on Asteroid TV study array at 100K

Figure 5 shows the typical spectral QE measured on an Asteroid TV study detector cooled at 100K, using the monochromator light source. The array response to this light is compared to response recorded in the same configuration with a reference detector previously calibrated at ESA [4]. Plotted points are the mean values of ratio of the tested Asteroid detector and the reference detector multiplied by the reference detector QE. Uncertainty is represented by grey lines, dominated by the imperfect knowledge of the reference detector QE. This spectral QE shows the expected cutoff wavelength around 2.1µm, as well as the cuton around 0.8µm expected from a device where the CdZnTe substrate is not completely removed. In the detection spectral band, the measured QE is between 70 and 90% suitable for astronomical needs.

4. DARK CURRENT

Dark current is then measured closing all sources of light in the cryostat. Without light, the dark charges are un-biasing progressively the photodiode resulting in a slowly increasing integration ramps. A linear regression performed on such a ramp gives an estimation of the slope, which is then interpreted as dark current. Figure 6 gives a colored mapping of the 4Mpx dark currents expressed in e/s (left) and dark current histogram (right) for the ALFA device à 100K. The resulting dark current appears very low, peaking at 0.002 e/s, ie approximately one electron every ten minutes! A tail toward higher dark current however still exists, spatially signed, but even with this tail, a vast majority of pixel are compliant with ESA requirement (0.1 e/s).

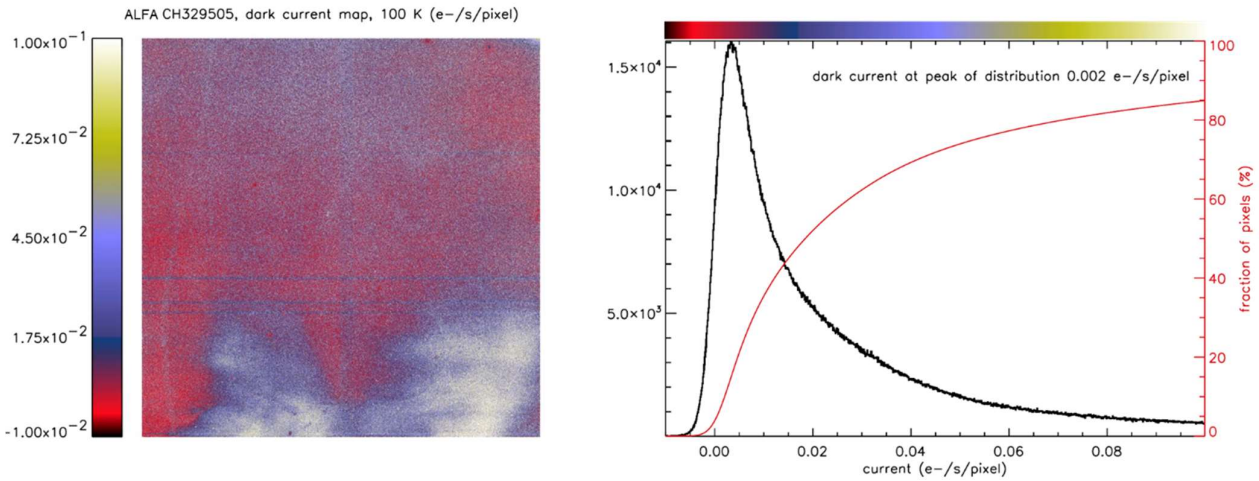

Figure 6: Dark current measured on the 4Mpx ALFA device at 100K,
Left: spatial mapping of the 2kx2k, Right: histogram on the 4Mpx

Repeating this measurement at different temperatures is instructive to investigate the source of this remaining dark current. Figure 7 presents the evolution of the peak dark current with temperature ranging from 80 to 200K. Three different devices are shown on this plot. An Asteroid TV study array, the first ALFA 2kx2k produced (ALFA #1) and the last one (ALFA #2, also called ALFA CH329505 in previous figures). Note that three years separates the fabrication of device ALFA#1 and device ALFA#2 at LETI. During those three years, LETI has been optimizing diode processing, in order to improve array performance. Note also that the diode process has been transferred to Lynred resulting in the Asteroid study array fabricated at Lynred and shown here.

As expected, dark currents decrease exponentially with temperature. At high temperature, all three devices seem to gather around the same values, following an exponential trend line with 362meV activation energy. This value is close to mid gap, suggesting a depletion limited generation mechanisms (2.1µm device mid gap is closer to 300meV). At lower temperatures however, the behavior tends to deviate from this exponential trend line, with dark currents that appear to be a little higher than expected. The difference is particularly obvious between the two ALFA arrays, emphasizing the progresses done at LETI to improve the diode performance: Only the coldest point at 100K from ALFA#2 deviates slightly (by a factor of 2) from the exponential trend line. Asteroid device from Lynred stays, exhibits also very good dark performances as it leaves this exponential trend line only at 110K and below.

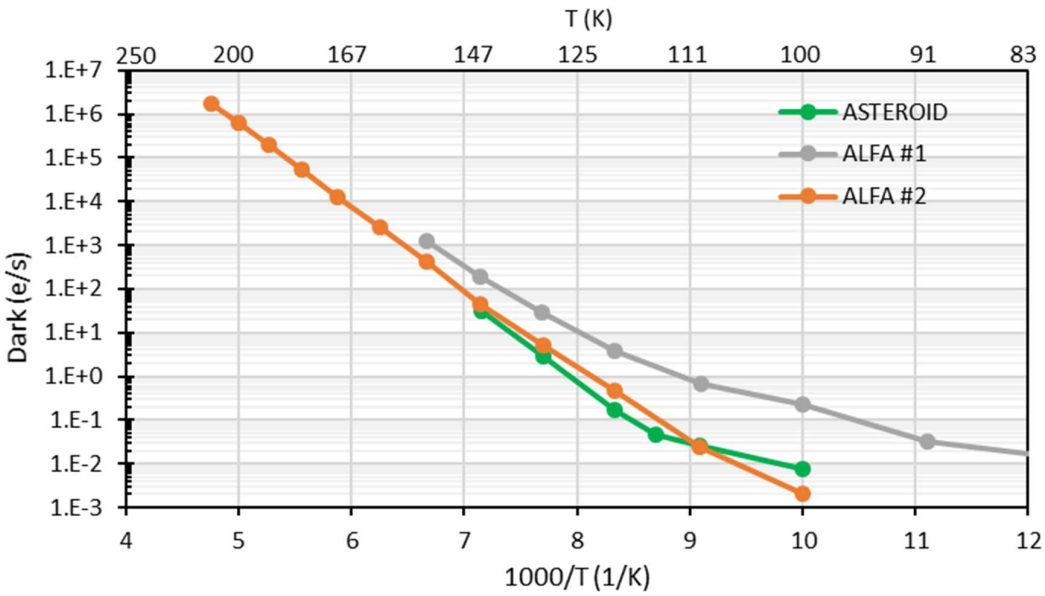

Figure 7: Thermal evolution of the measured dark current on both Asteroid TV array and ALFA 2kx2k array

5. IPC AND PERSISTENCE

Now that first order figures of merit (FOM) have been validated on this technology (QE on study TV array, and dark current onto the large area of a 2kx2k focal plane array), the next paragraphs will be more focused in second order FOMs such as interpixel capacitance (IPC) or persistence.

IPC is an important FOM for SFD based arrays. Indeed, the charge integration occurs onto de photodiodes capacitance, which means that the photodiode contact bias will vary during the integration. If two neighboring pixels are coupled through capacitive coupling, a part of their integrated charges will be shared between them thus degrading the imagine properties of the array. The TV ROIC used in study array is equipped with a specific feature in order to assess this IPC: 96 pixels ventilated evenly onto the array surface can be maintained at reset bias while the rest of the pixels are integrating. Therefore, in this operation mode, the ratio between the IPC pixels and their nearest neighbors gives an estimation of the IPC. Figure 8 gives an example of such a measurement. The normalization to the central pixel gives therefore a direct estimation of lateral coupling: for each IPC pixel, the nearest neighbor exhibit larger values than further pixels. Figure 8 left shows an example of the resulting relative mapping around an IPC pixel, for a 900mV reset bias at 90K on an Asteroid device processed at LETI. A cross shape is clearly visible around the IPC central pixel, indicating a 0.5% pixel lateral coupling. At the end the total IPC (sum of the four nearest neighbors) peaks around 2.5% when considering the 96 IPC dedicated pixels available onto the array, with no clear spatial signature (white spatial distribution). This value is within ESA specifications (3%).

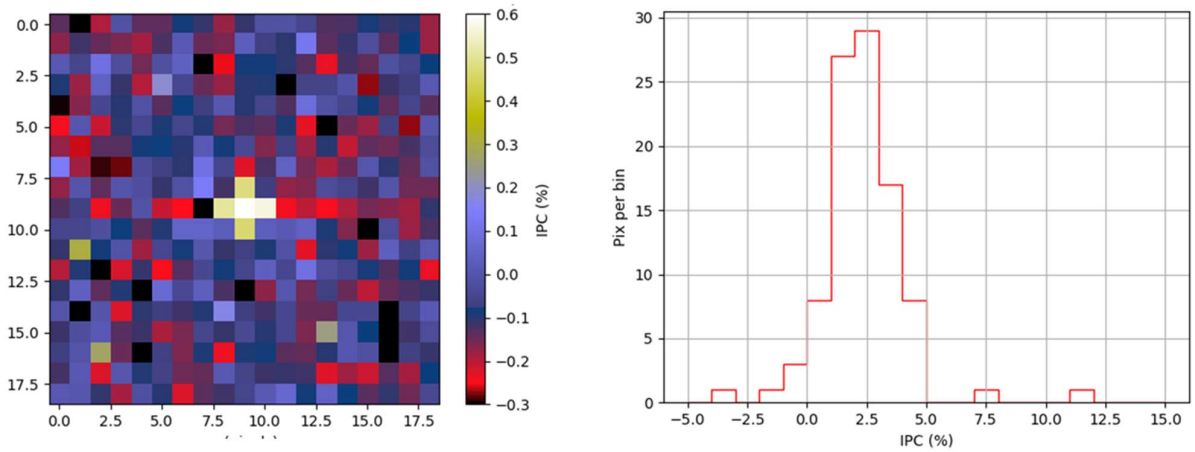

Figure 8: Example of an IPC measurement using dedicated pixels available (Asteroid study array at 90K)
Left: Example of an IPC relative mapping
Right: Histogram of the total IPC measured on the 96 available pixels)

Furthermore, persistence appears as a major limitation for astronomy observations. In few words, when such a detector is observing a given flux scene, and then immersed into darkness, trapping-detrapping of the photo-charges in the detector structure occurs so that the ghost of the previous image remains visible onto the detector output image. This effect is poorly documented in the literature, each characterization team using its own methodology to characterize/calibrate it. In [5], ESO team demonstrated that most of the time, optical stimulus of this persistence is similar to electrical stimulus (the pixel bias is changed directly using the ROIC itself instead of letting it drift integrating photo-charges). The full discussion may be found in [6] and [7]. Using this electrical stimulation protocol, LETI and Lynred technology have been compared using study arrays.

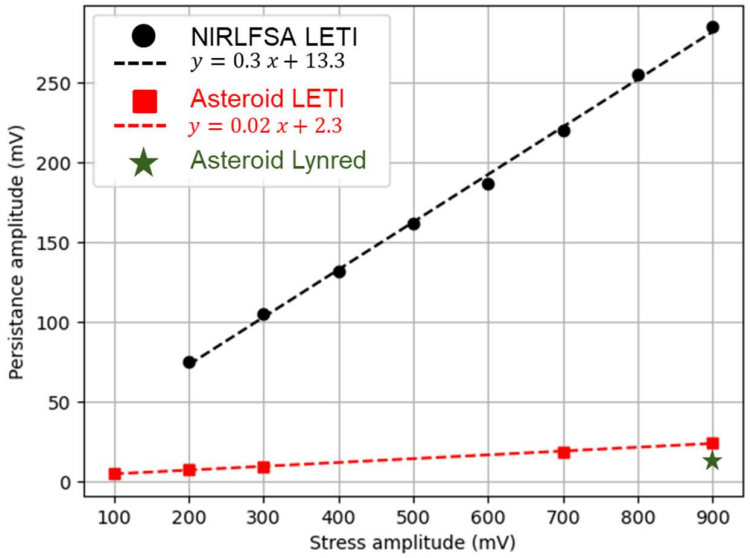

Figure 9: Persistence measured with electrical stress on three study arrays from LETI and Lynred

Figure 9 shows this comparison. The plot includes measurements performed on a pre-ALFA array processed at LETI in 2018 (study array used during the qualification phase of the ALFA project). Different levels of electrical stimulus are used and results in a persistence output linear with the stimulus. Figure 9 gathers also measurements performed on an Asteroid array processed at LETI as well as an Asteroid array processed at Lynred. Both arrays exhibit much lower persistence levels than the very first array: the technology optimization does not only improve dark current but also persistence.

6. FIRST IRRADIATIONS

Using study array from the pre-ALFA demonstration phase, we have also been working on the understanding of the behavior of such a technology under irradiation. The first work was focused on the interaction of irradiation protons with the CZT substrate. Indeed, some previous work on Teledyne's H1RG showed a degradation of the dark current mapping without CZT thinning [8]. Using modeling and an experimentation validation campaign, we were able to demonstrate that this effect is in fact due to the luminesce of high-energy electrons deposited by the irradiation protons. Those high energy electrons may either diffuse toward the narrow gap layer and be finally collected by the photodiodes, or relax emitting photons at the CZT substrate gap and then propagate toward the MCT sensitive layer to be detected. Both processes end up polluting the detected images [9]. As a result, during irradiation, even under darkness, the measured dark current is higher than expected. Figure 10 shows dark current measurements performed during 36MeV proton irradiation at very low flux (<100 p+/s/cm²) on two study arrays with different CZT substrate thicknesses (50 and 800µm). Arrays were partly shielded during irradiation to be able to easily estimate the effect of the irradiation. It appeared that 800µm CZT left leads to a significant increase of the apparent dark current due to luminescence in the substrate, whereas thinning the substrate down to 50µm, no difference between shielded and unshielded area was seen. This result is confirmed by the modeling of the proton interaction with CZT substrate associated luminescence and carrier diffusion showing that the luminescence dominates the process [10].

At the end of this first irradiation campaign, a dose of 1e9 p/cm² has been reached. After one thermal cycle to ambient temperature, no harm was seen on the detector, in terms of dark current or even persistence. Further irradiation campaigns are planned to assess the radiation hardness of such a technology up to higher doses.

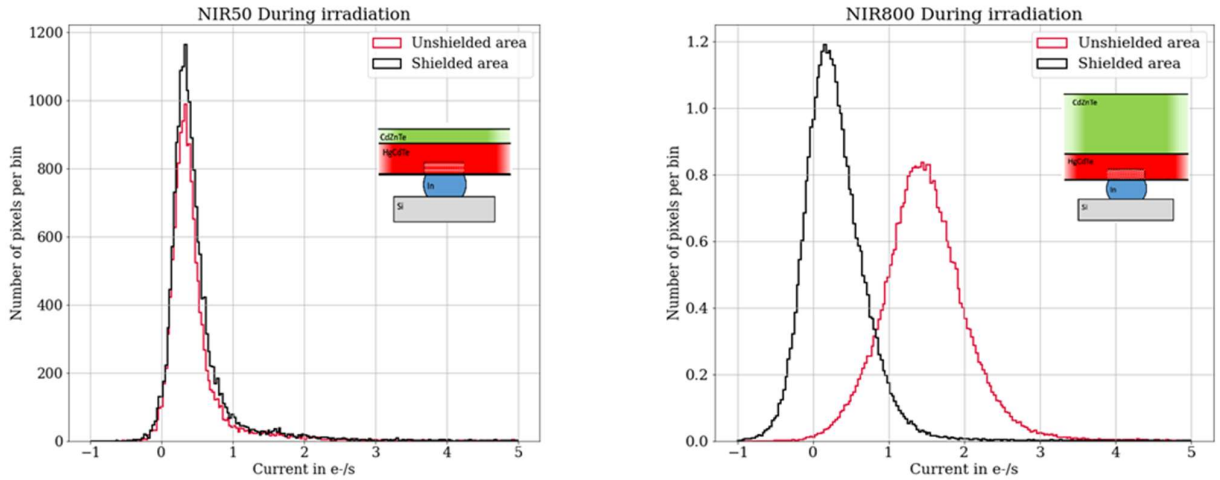

Figure 10: Dark current histograms measured during 36MeV irradiation protons, for two substrate-thinning configurations: Left: 50µm CZT substrate, Right: 800µm CZT left.

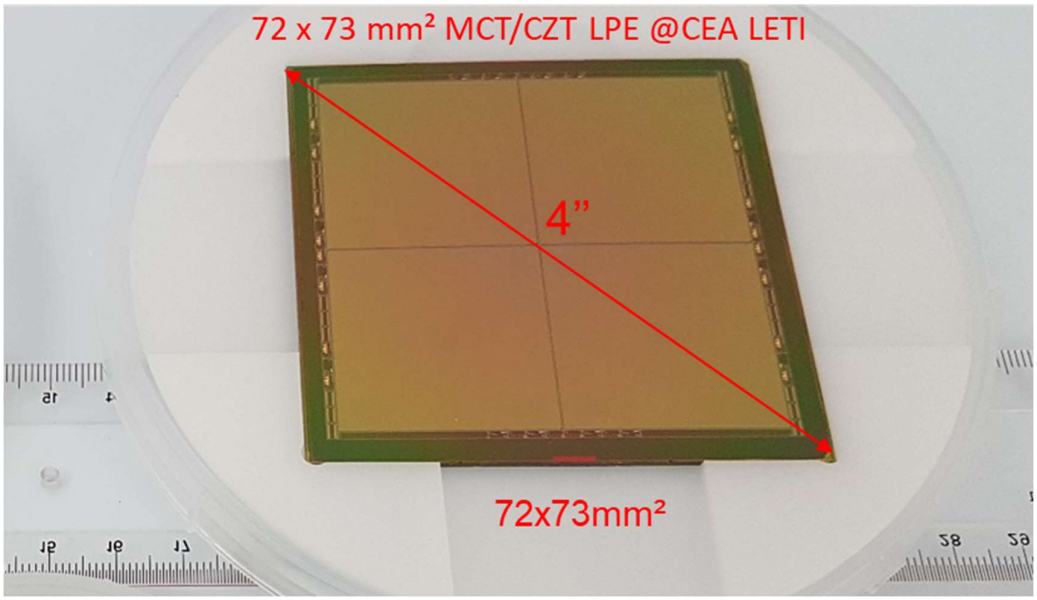

Figure 11: First demonstration of a 4’’ process to fit four 2kx2k arrays onto a single wafer

7. CONCLUSION AND PERSPECTIVES

We demonstrated the ability to build high performance $2k \times 2k$ 15µm pitch array in the NIR range ($\lambda_c = 2.1\mu m$) for astronomy needs. Sensitive MCT layer was grown and processed at CEA-LETI, while ROIC hybridization and packaging were carried out at Lynred. Finally, large array characterization was done at CEA-IRFU. First order FOMs are validated with high QE (between 70 and 90% depending on the wavelength) and very low dark currents (2e-3 e/s/pixel at 100K). Interpixel capacitance was also validated on study array, with a total 2.5 % IPC with the four neighboring pixels. Moreover, persistence measurements were also studied, demonstrating a significant improvement with

technology optimization. Finally, radiation hardness is currently being evaluated. First proton irradiation results showed no main issues with this technology. The last array manufactured will be installed onto the CAGIRE IR camera in the Éclair instrument to be used within the SWOM mission [11, 12].

In parallel to this ALFA demonstration program, LETI and Lynred is working onto the industrialization phase of such large format array, in the frame of the Asteroid Europe H2020 program. The main issue is to set up a large format processing chain (CZT substrate growth, LPE of the MCT narrow gap absorbing layer, diode processing, dicing and packaging). As an example, Figure 11 shows a 4 inch MCT/CZT processed layer, exhibiting four ALFA 2kx2k arrays onto the same wafer. This ongoing effort is not dedicated only to large format arrays (such as ALFA) but is expected to be useful for the whole MCT fabrication chain in order to improve production throughput.

ACKNOWLEDGMENTS

This work is a fruitful collaboration between CEA LETI, CEA IRFU and Lynred with ESA (NirLFSA), H2020 (Asteroid) and ANR (Labex Focus ANR-11-LABX-0013)

REFERENCES

[1] Cervera, C., Boulade, O., Gravrand, O. et al. (2017), *"Ultra-Low Dark Current HgCdTe Detector in SWIR for Space Applications*". J. Electron. Mater. 46, 6142–6149. https://doi.org/10.1007/s11664-016-4936-0

[2] Fièque, B., Martineau, L., Sanson, E., Chorier, P., Boulade, O., Moreau, V., & Geoffray, H. (2011). « *Infrared ROIC for very low flux and very low noise applications*". SPIE, 8176, 81761I-81761I – 13. https://doi.org/10.1117/12.898987

[3] Gravrand, O., Ballet, P., Baylet, J., & Baier, N. (2009). "*HgCdTe p-on-n focal-plane array fabrication using arsenic incorporation during MBE growth*". Journal of Electronic Materials, 38(8), 1684–1689. https://doi.org/10.1007/s11664-009-0794-3

[4] Gooding D., Crouzet P.E., Duvet L., Prod'homme T., Smit H., Ter Haar J., Blommaert S., Visser I., Lemmel F., Heijnen J. , Van Der Luijt C., Butler B., Beaufort T. (2016) "*Large format array NIR detectors for future ESA astronomy missions: characterization and comparison*", SPIE 99151G, https://doi.org/10.1117/12.2231179

[5] Simon Tulloch, Elizabeth George, et al (2019), "P*redictive model of persistence in H2RG detectors*", Journal of Astronomical Telescopes, Instruments, and Systems 5(3), 036004, https://doi.org/10.1117/1.JATIS.5.3.036004

[6] . Le Goff T., Pichon T., Baier N., Gravrand O., Boulade O.,(2022) «*Model and characterization of persistence in HgCdTe SWIR detectors for astronomy applications*", To be published in Journal of Electrical Material.

[7] Titouan Le Goff (2022), *« Etude de la persistance dans les rétines proches IR en HgCdTe pour les applications en astronomie* », thèse.

[8] Smith R., Bebek C. Bonati M., Brown M.G., Cole D. et al. (2006) « *Noise and Zero point drift in 1.7um cutoff detectors for SNAP*», Proceeding of SPIE 62760R , https://doi.org/10.1117/12.672616

[9] Thibault Pichon (2020), « *Modélisation et caractérisation expérimentale du phénomène de luminescence induit par l'irradiation de protons dans les détecteurs IR HgCdTe en environnement spatial* », Thèse

[10] Pichon, T., Mouzali, S., Boulade, O. et al., (2020), « *Influence of the CdZnTe Substrate Thickness on the Response of HgCdTe Detectors Under Irradiation: Modeling of the Substrate Luminescence*". J. Electron. Mater. 49, 6918–6935. https://doi.org/10.1007/s11664-020-08237-0

[11] D. Corre et al., (*2018*), « *End-to-end simulations for COLIBRI, ground follow-up telescope for the SVOM mission* », vol. 10705. doi: 10.1117/12.2313127

[12] J. Fuentes-Fernández et al., (2020), « *Optical Design of COLIBRÍ: A Fast Follow-up Telescope for Transient Events*», J. Astron. Instrum., vol. 09, no 01, p. 2050001, mars, doi: 10.1142/S2251171720500014